ELSEVIER

Contents lists available at ScienceDirect

International Journal of Biological Macromolecules

journal homepage: www.elsevier.com/locate/ijbiomac





Preparation of MIL100/MIL101-alginate composite beads for selective phosphate removal from aqueous solution

Eric Alvares ^{a, 1}, Stanley Tantoro ^{a, 1}, Christian Julius Wijaya ^{a, b}, Kuan-Chen Cheng ^{c, d, e, f, *}, Felycia Edi Soetaredjo ^{a, b}, Hsien-Yi Hsu ^{g, h}, Artik Elisa Angkawijaya ⁱ, Alchris Woo Go ^j, Chang-Wei Hsieh ^{k, l}, Shella Permatasari Santoso ^{a, b, **}

- ^a Chemical Engineering Department, Widya Mandala Surabaya Catholic University, Surabaya 60114, East Java, Indonesia
- ^b Collaborative Research Center for Zero Waste and Sustainability, Jl. Kalijudan 37, Surabaya 60114, East Java, Indonesia
- c Institute of Food Science and Technology, National Taiwan University, #1, Sec. 4, Roosevelt Rd., Taipei 10617, Taiwan
- d Institute of Biotechnology, National Taiwan University, #1, Sec. 4, Roosevelt Rd., Taipei 10617, Taiwan
- e Department of Medical Research, China Medical University Hospital, China Medical University, 91, Hsueh-Shih Road, Taichung 40402, Taiwan
- f Department of Optometry, Asia University, 500, Lioufeng Rd., Wufeng, Taichung 41354, Taiwan
- g School of Energy and Environment, Department of Materials Science and Engineering, City University of Hong Kong, Kowloon Tong, Hong Kong, China
- ^h Shenzhen Research Institute of City University of Hong Kong, Shenzhen 518057, China
- ⁱ Center for Sustainable Resource Science, RIKEN, Yokohama 230-0045, Japan
- ^j Department of Chemical Engineering, National Taiwan University of Science and Technology, Taipei 10607, Taiwan
- k Department of Food Science and Biotechnology, National Chung Hsing University, South Dist., Taichung City 40227, Taiwan
- Department of Medical Research, China Medical University Hospital, North Dist., Taichung City 404333, Taiwan

ARTICLE INFO

Keywords: Phosphate adsorption Hard soft acid base theory MOF-alginate composite

ABSTRACT

Numerous studies have reported various approaches for synthesizing phosphate-capturing adsorbents to mitigate eutrophication. Despite the efforts, concerns about production cost, the complexity of synthesis steps, environmental friendliness, and applicability in industrial settings continue to be a problem. Herein, phosphate-selective composite adsorbents were prepared by incorporating alginate (Alg) with MIL100 and MIL101 to produce the MIL100/Alg and MIL101/Alg beads, where Fe^{3+} served as the crosslinker. The unsaturated coordination bond of MIL100 and MIL101 serves as a Lewis acid that can attract phosphate. The adsorption equilibrium isotherm, uptake kinetics, and effects of operating parameters were studied. The phosphate adsorption capacity of MIL100/Alg (103.3 mg P/g) and MIL101/Alg (109.5 mg P/g) outperformed their constituting components at pH 6 and 30 °C. Detailed evaluation of the adsorbent porosity using N₂ sorption reveals the formation of mesoporous structures on the Alg network upon incorporation of MIL100 and MIL101. The composite adsorbents have excellent selectivity toward anionic phosphate and can be easily regenerated. Phosphate adsorption by MIL100/Alg and MIL101/Alg was driven by electrostatic attraction and ligand exchange. Preliminary economic analysis on the synthesis of the adsorbents indicates that the composites, MIL100/Alg and MIL101/Alg, are economically viable adsorbents.

1. Introduction

Phosphorous (P), along with nitrogen (N) and potassium (K), is an essential nutrient for the growth of healthy crops [1,2]. The supplementation of these nutrients to agricultural land is known to benefit the crop yield [3–5], which then leads to their immense consumption. In

2000, 20.64 million metric tons (MT) of P fertilizer were spent in arable lands globally, and its usage increased to 30 million MT by 2019 (see Supplementary Information, Fig. S1a) with China as the largest user, followed by India, Brazil, and the United States (Fig. S1b). Different crops are postulated to require different amounts of P (Fig. S1c) [3]. Despite this knowledge, fertilizer supplementation is often done in

^{*} Correspondence to: K.-C. Cheng, Institute of Food Science and Technology, National Taiwan University, #1, Sec. 4, Roosevelt Rd., Taipei 10617, Taiwan.

^{**} Correspondence to: S. P. Santoso, Chemical Engineering Department, Widya Mandala Surabaya Catholic University, Surabaya 60114, East Java, Indonesia. *E-mail addresses*: kccheng@ntu.edu.tw (K.-C. Cheng), shella@ukwms.ac.id (S.P. Santoso).

¹ The authors are contributed equally to this work.

excess to ensure that plants have the required macronutrients. On average, only 20 % of available P is taken up and assimilated by the plants (Fig. S1d), while the unabsorbed P pollutes eventually leach to the water bodies triggering the downstream eutrophication hazard [3–6].

According to the National Pollutant Discharge System by the US Environmental Protection Agency (EPA), many municipal wastewater treatment facilities were not equipped with the technology to treat excess P. The lack of such systems may be due to the high complexity and cost required for P removal. To alleviate the burden of the pollutant, P-contaminated water can be restored using biological, chemical, or physical treatment approaches [6-8]. A moving bed biofilm reactor (MBBR) is commonly used to treat N- and P-contaminated water biologically [10]. However, multiple-stage treatment to ensure the treated waters meet discharge requirements and acidification of the wastewater must be done prior to the MBBR treatment, which eventually entails additional cost and maintenance. P removal could be done chemically alongside the removal of suspended solids by flocculants addition (e.g., polyaluminum chloride and FeCl₃) [9]. Despite its effectiveness, this method was deemed impractical for treating concentrated pollutants due to the generation of chemical sludge in large amounts. For polluted waters with high concentrations of P, physical treatments like adsorption would be favorable. Adsorption can be used as a pretreatment step to reduce the P levels before adopting the methods mentioned above as polishing steps. However, with appropriate operating conditions and choice of adsorbent, adsorption can be used as a sole treatment process to reduce the P in contaminated waters to the permitted level. Adsorption as a treatment method is preferred given its versatility to remove a wide range of contaminants with the appropriate adsorbent, ease of operation, and low operating costs. Since treating contaminated water or wastewater is a resource-consuming yet non-income-generating process, efforts should be directed toward developing straightforward processes alongside strategies that would provide positive economic gains when establishing treatment systems for P removal.

The choice of adsorbent in the adsorption process is crucial as it dictates the overall effectiveness of the treatment processes. Thus, it is imperative to consider the properties of the adsorbate in choosing and designing an effective adsorbent [10-15]. Various adsorbents derived from synthetic or natural materials have been developed for P adsorption. Different strategies have also been employed to increase the adsorbent's affinity for P. Since P tends to form anionic species in solution, the immobilization of positively charged metal ions can promote electrostatic attraction, improving the adsorbate-adsorbent interaction [16-20]. For example, adding the cationic tetravalent Zr to chloromethyl styrene grafted polyethylene-coated polypropylene fibers resulted in an adsorbent with a positively charged surface. The polymeric fibers were demonstrated to have a good affinity for anionic phosphate (Pi) with an adsorption capacity of 10.55 mg of Pi, equivalent to 3.44 mg of P per g of adsorbent [18]. While immobilizing metal ions may increase the P adsorption capacity of the adsorbent, the metal in its ionic form may leach into the solution. To prevent possible leaching, immobilization of the metal as part of a metal-organic framework (MOF) is one solution. Shahat et al. [21] demonstrated cationic surfactant and ammonium molybdate surface-modified UiO-66 for P adsorption; the maximum adsorption capacity was reported to be 70.47 mg of Pi (23.00 mg of P) per g. By adopting the latter strategy, where MOF was used as the adsorbent to remove P from water —herein, iron-based MOFs (Fe-MOFs), namely MIL100 and MIL101 were implemented. Fe-MOFs have an excellent interaction affinity toward P [22,23]. According to the hard-soft acid-base (HSAB) principle, compounds with the same extrinsic properties will have strong affinity. In this case, both P and Fe are classified as strong bases and strong acids, so they may exhibit strong affinity toward one another.

Besides good adsorption performance, the ease of handling is an added value for adsorbents. Hydrogel adsorbents may deliver a more facile separation and retrieval than the powdered form. Alginate is a

natural polysaccharide widely used for preparing adsorbents because of its ease of modification [24]. Alginates can be converted into hydrogels by simple crosslinking reactions with multivalent metal ions, such as ${\rm Ca}^{2+}$ and ${\rm Fe}^{3+}$ [25,26]. In addition, alginates have the advantages of being environmentally friendly, widely available, and inexpensive [27,28]. The presence of ${\rm Fe}^{3+}$ in alginate is in line with the previously mentioned HSAB principle, which could potentially improve the adsorption of Pi. Therefore, it is of interest to look into the integration of Fe-MOFs into alginate hydrogel and its performance as an adsorbent for Pi.

MIL100 and MIL101 were prepared in this work and subsequently grafted into alginate-based hydrogels; Fe^{3+} ions are used to initiate the hydrogel formation and as a crosslinker. Alginate hydrogels grafted with MIL100- and MIL101 (denoted as MIL100/Alg and MIL101/Alg) were then used for P adsorption in aqueous solutions. The said adsorbents have not been extensively studied in the past. The adsorbed P was calculated as the total Pi adsorbed; which represents the total anionic species H_3PO_4 , H_2PO_4 , HPO_4^{2-} , and PO_4^{3-} . This study aimed to evaluate the adsorption mechanism and behavior of the MIL100/Alg and MIL101/Alg in removing Pi from P-contaminated waters. The specific objectives include (i) characterization of the adsorbent before and after adsorption, (ii) establishing the kinetic profile and equilibrium isotherm of the adsorption process using the alginate-based hydrogels grafted with Fe-MOFs, (iii) evaluating the effect of pH, initial adsorbate concentration, and coexisting ions on the equilibrium uptake of Pi by the alginate-based hydrogels grafted with Fe-MOFs, and (iv) evaluating the reusability and production cost of the Fe-MOF-grafted alginate hydrogels.

2. Materials and method

2.1. Chemicals

Sodium alginate with a viscosity of 5 to 40 cps was purchased from CV Nura Jaya, a chemical distributor in East Java, Indonesia. FeCl $_3$ ·6H $_2$ O (99 % purity) was obtained from SAP Chemical. 1,3,5-Benzenetricarboxylic acid ($C_9H_6O_6$, 95 % purity), nitric acid (HNO $_3$, 65 % purity), dimethylformamide (C_3H_7NO , 99 % purity), terephthalic acid ($C_8H_6O_4$, 99 % purity), ethanol (C_2H_6O , 99 % purity), antimony potassium tartrate (K(SbO)C $_4H_4O_6$ ·1/2H $_2O$, 99 %), ascorbic acid ($C_6H_8O_6$, 99.7 % purity), 1,10-phenanthroline ($C_{12}H_8N_2$, 99 % purity) and ammonium heptamolybdate ((NH $_4$) $_6Mo_7O_{24}$, 82 % purity) were obtained from Merck, Germany. Sodium phosphate dibasic dihydrate (Na $_2$ HPO $_4$ ·2H $_2$ O, 99 % purity) and Polysorbate 20 were obtained from Sigma Aldrich, USA. All chemicals were used as received without further purification. The solution used in this study was prepared using reverse osmosis water with a total dissolved solids concentration of 10–20 ppm.

2.2. Experimental procedure

2.2.1. Preparation of Fe³⁺-crosslinked alginate hydrogel

The Fe $^{3+}$ -crosslinked alginate (Alg) was prepared by dissolving 3 wt % of sodium alginate in water. The solution was stirred for an hour at 50 °C to obtain a homogenous alginate solution. The alginate solution was taken using a 1000 μ L micropipette and then dripped drop-by-drop in 0.05 M FeCl $_3$ solution. The resultant hydrogel beads were left in the FeCl $_3$ solution for 12 h to ensure the complete crosslinking of the alginate chain by Fe $^{3+}$. The crosslinked beads were collected and dried in a 70 °C oven overnight. The dried beads were spherical and predominantly 2.3 mm in diameter (Fig. S2a).

2.2.2. Preparation of MIL100/Alg and MIL101/Alg

The preparation procedure for the MOF powders (i.e., MIL100 and MIL101) was based on the reports by Simon et al. [29] and Wang et al. [5], respectively. These powders were then used to prepare MIL100/Alg and MIL101/Alg hydrogel beads. Briefly, 3 wt% of sodium alginate was

stirred for an hour in 50 $^{\circ}$ C water to obtain the clear alginate solution. Subsequently, 100 mg of MIL100 or MIL10 and 0.1 wt% of Polysorbate 20 were added into the alginate solution kept in 50 $^{\circ}$ C under a constant stirring for 4 h. Hydrogel beads were formed from the solution mixture using the same technique to prepare Alg. The dried hydrogel beads of MIL100/Alg and MIL101/Alg have diameter size predominantly 2.4 mm (Fig. S2b and c).

2.2.3. Adsorbent characterization

Fourier transform infrared (FTIR) spectroscopy analysis was conducted using a Shimadzu IRTracer-100, and KBr was used as the background. X-ray diffraction (XRD) pattern of the samples was collected using a Bruker D2 Phaser X-ray diffractometer with $\text{CuK}\alpha$ radiation. N_2 sorption isotherm was performed using a BEL-Belsorp Max analyzer, and the samples were degassed at 423 K for 6 h before analysis. The swelling percentage (%swelling) of the materials was measured by immersing the dried hydrogel beads for a specific time in the water. The %swelling was calculated by using Eq. (1).

%swelling =
$$100\% + \left(\frac{m_{\text{wet}} - m_{\text{dry}}}{m_{\text{dry}}} \times 100\%\right)$$
 (1)

where $m_{\rm wet}$ and $m_{\rm dry}$ are the mass of hydrogel beads after and before water immersion.

2.2.4. Adsorption study

2.2.4.1. Effect of parameters. The stock Pi solution was prepared by dissolving $Na_2HPO_4\cdot 2H_2O$ in water at 1000 mg Pi/L concentration. A series of 10 mL diluted Pi solutions at a concentration of 300 mg/L was prepared from the stock solution. The pH of each solution was adjusted from 4 to 9 by adding 0.1 M of HCl or NaOH solution. Subsequently, adsorbent at a dose of 2.5 g/L was added to the Pi solution and left under constant shaking for 8 h at a constant temperature of 30 °C. The residual Pi concentration was determined by employing a colorimetric procedure using a molybdate reagent; the detailed procedure can be found elsewhere [30].

2.2.4.2. Adsorption isotherm. A series of 10 mL Pi solutions at different initial concentrations were prepared, i.e., 30 to 600 mg/L. The pH of each solution was adjusted to 6. Subsequently, adsorbent at a dose of 2.5 g/L was added to the Pi solution, and the adsorption was conducted for 8 h at a specific constant temperature (i.e., 30, 40, and 50 °C). The residual Pi concentration was determined by the aforementioned colorimetric procedure. The equilibrium adsorption capacity (Q_e , mg/g) is calculated according to Eq. (2)

$$Q_e = \frac{C_0 - C_e}{m} \times V \tag{2}$$

where C_0 is the initial Pi concentration (mg/L), C_e is the residual adsorbate concentration at equilibrium (mg/L), m is the mass of adsorbent (g), and V is the volume of solution (L).

2.2.4.3. Adsorption kinetic. A series of 10 mL Pi solutions were prepared at an initial concentration of 300 mg/L. Subsequently, the adsorbent was added to the Pi solution at a dose of 2.5 g/L. The Pi's residual concentration was measured using the colorimetric procedure at a predetermined time. The time-dependent adsorption capacity (Q_t , mg/g) can be calculated using Eq. (2), by replacing the subscript "e" which refers to the equilibrium state to "t" which refers to the state at a given time.

2.2.5. Recyclability and Pi release study

The regeneration of the spent-adsorbent, i.e., adsorbent, which has been used for Pi adsorption, was done by immersing the adsorbent in a pH 9 solution for 24 h. The regenerated adsorbent was collected, rinsed

with water, and dried in a 70 $^{\circ}$ C oven overnight. Then, the adsorbent was reused for another adsorption process. The desorption-adsorption was done in three cycles. In addition, the Pi release study was performed by immersing the spent adsorbent in 1000 mL water in a clear flask. Then, the flask was put under direct sunlight for 6 h, and the amount of Pi released was measured each hour to determine the cumulative Pi release.

2.3. Adsorption modeling

Isotherm modeling was performed by applying Langmuir, Freundlich, Frumkin-Fowler-Guggenheim, and Dubinin-Randushkevich [7,31]. The Langmuir model has the following mathematical expression:

$$Q_{\rm c} = \frac{Q_{\rm L,max} K_{\rm L} C_{\rm c}}{1 + K_{\rm L} C_{\rm c}} \tag{3}$$

$$R_{\rm L} = \frac{1}{1 + K_{\rm I} C_0} \tag{4}$$

where $Q_{\rm L,\ max}$ is the maximum adsorption capacity (mg/g), $K_{\rm L}$ is an equilibrium constant related to adsorption affinity (L/mg), and $R_{\rm L}$ is a dimensionless separation factor.

The Freundlich model can be expressed as the following mathematical expression:

$$Q_{\rm e} = K_{\rm F} C_{\rm e}^{1/n_{\rm F}} \tag{5}$$

where K_F is an equilibrium constant ((mg/g)(mg/L)^{$-n_F$}), and n_F is a dimensionless parameter related to the favorability of the adsorption process.

The Frumkin-Fowler-Guggenheim can be employed by following the mathematical expression:

$$Q_{\rm e} = \frac{Q_{\rm FFG} K_{\rm FFG} C_{\rm e} exp(-\varphi)}{1 + Q_{\rm FFG} K_{\rm FFG} C_{\rm e} exp(-\varphi)} \tag{6}$$

$$\varphi = \frac{2\omega\theta}{RT} = \frac{2\omega}{RT} \frac{Q_{\rm c}}{Q_{\rm FFG}} \tag{7}$$

where $Q_{\rm FFG}$ is the maximum adsorption capacity (mg/g), $K_{\rm FFG}$ is an equilibrium constant (L/mg), ω is a parameter related to the heat of adsorption (kJ/mol), and θ is the fractional coverage.

The Dubinin-Randushkevich model expresses as follows:

$$Q_{\rm e} = Q_{\rm DR} exp(-B_{\rm DR} \varepsilon^2) \tag{8}$$

$$\varepsilon = RT \ln \left(1 + \frac{1}{C_{\rm c}/C_{\rm s}} \right) \tag{9}$$

$$E_{\rm DR} = \frac{1}{\sqrt{2B_{\rm DR}}}\tag{10}$$

where $Q_{\rm DR}$ is the maximum adsorption capacity (mg/g), $B_{\rm DR}$ is the constant related to the energy of adsorption (mol²/kJ²), ε is the constant related to the adsorption potential (kJ/mol), R is the gas constant (8.314 J/mol K), T is the adsorption temperature (K), $C_{\rm s}$ is the adsorbate solubility (mg/L), and $E_{\rm DR}$ is the adsorption energy (kJ/mol).

The adsorption kinetic data were modeled using Pseudo-first-order, Pseudo-second-order, Elovich, and intra-particle diffusion models [32]. The mathematical expression of the Pseudo-first-order and Pseudo-second-order models is expressed by Eqs. (11) and (12), respectively.

$$Q_{t} = Q_{e,1} \left(1 - e^{-k_1 t} \right) \tag{11}$$

$$Q_{t} = \frac{Q_{c,2}^{2} k_{2} t}{1 + Q_{c,2} k_{2} t}$$
 (12)

where $Q_{e, 1}$ and $Q_{e, 2}$ represent the equilibrium amount of Pi uptake (mg/g); k_1 and k_2 are the adsorption rate constant with the unit of 1/min and mg/g min, respectively, and t is the adsorption time (min).

The Elovich and intra-particle diffusion model is expressed by Eqs. (13) and (14), respectively.

$$\frac{Q_{\rm t}}{Q_{\rm ref}} = R_{\rm E} l n \frac{t}{t_{\rm ref}} + 1 \tag{13}$$

$$\frac{Q_{\rm t}}{Q_{\rm ref}} = 1 - R_{\rm i} \left(1 - \frac{t}{t_{\rm ref}} \right)^{1/2} \tag{14}$$

where $Q_{\rm ref}$ is the adsorption capacity at $t_{\rm ref}$ (mg/g); $t_{\rm ref}$ is the operating time at which the equilibrium condition in the system is reached; in this case $t_{\rm ref}$ is assumed to be the longest operating time; $R_{\rm E}$ and $R_{\rm i}$ are dimensionless equilibrium parameters used to describe the characteristic of the adsorption profile.

3. Results and discussion

3.1. Adsorbent characterization

3.1.1. N₂ sorption isotherm

Fig. 1 shows the N₂ sorption isotherms of MIL100/Alg and MIL101/ Alg, the adsorption and desorption isotherms for MIL100 and MIL101 are provided in Fig. S3b for comparison. The occurrence of adsorption at $p/p_0 \rightarrow 0$ for MIL100 and MIL101 indicates the microporous structure [33]. A slit hysteresis loop was observed at $p/p_0 \sim 0.6$ for MIL100 and p/ $p_0 \sim 0.4$ for MIL101, indicating the presence of a mesoporous structure. The dominancy of the microporous structure for MIL100 and MIL101 is also shown from the pore distribution curve in the inset Fig. S3b, where the highest peak occurred at pore radius ~ 1 nm. As for the MIL100/Alg and MIL101/Alg (Fig. 1), the micropore filling region at $p/p_0 \rightarrow 0$ was smaller, implying the reduced micropore structure for the two materials. The appearance of the hysteresis loop starting from $p/p_0 \sim 0.4$ was becoming clearer for MIL100/Alg and MIL101/Alg, implying the dominance of mesoporous structure. The mesoporosity of MIL100/Alg and MIL101/Alg can also be noticed from the pore distribution, which is dominated at a radius of 2-18 nm (inset Fig. 1).

The calculated BET parameters based on the measured N_2 sorption isotherm are given in the supplementary information Table S1. The addition of the Alg matrix that envelops the MOF particles causes a decrease in the determined BET surface area ($a_{s,BET}$). In particular, Fe-MOF-grafted alginate hydrogels have significantly lower surface areas with $a_{s,BET}$ of 6.061 and 3.037 m²/g for MIL100/Alg and MIL101/Alg, respectively. In contrast, the free MIL100 and MIL101 have $a_{s,BET}$ of

387.8 and 201.8 m²/g, respectively. The low $a_{\rm s,BET}$ of MIL100/Alg and MIL101/Alg can be attributed to (i) the nonporous nature of Alg and (ii) an increase in pore size and/or a decreased number of pores. From the determined mean pore diameter (Table S1), MIL100/Alg and MIL101/Alg possess wider pores than MIL100 and MIL101, which consequently causes a decrease in the total pore volume and $a_{\rm s,BET}$.

3.1.2. X-ray diffraction pattern

The XRD patterns of MIL100/Alg and MIL101/Alg are given in Fig. S3a; XRD of the parent compounds, namely MIL100, MIL101, and Alg, is also provided for reference. The obtained XRD patterns of MIL100 and MIL101 are consistent with the reported literature [34,35], indicating the successful synthesis of these compounds. For MIL100, the diffraction peaks at 2-Theta of 2–5° have a slight decrease in intensity, which signify the decreased crystallinity. This can be influenced by the usage of different solvents for its synthesis [34], where HNO₃ solution is used instead of HF. The peaks corresponding to guluronic and manuronic moiety of sodium alginate were weakly observed for Alg, indicating the successful crosslinking of the alginate chains. The XRD pattern of MIL100/Alg and MIL101/Alg exhibit irregular and broad diffused peaks, which show the amorphous structure of the materials.

3.1.3. Functional groups of the adsorbents

The FTIR spectra of MIL100/Alg and MIL101/Alg before (fresh) and after (used) adsorption are presented in Fig. 2a. The spectra for parent compounds are provided in Fig. S4, and the corresponding peak wavenumber is summarized in Table S2. Zone I FTIR spectrum, highlighted in brown, of all fresh adsorbents can be attributed to $\nu(O-H)$; the peak intensity is reduced in the used adsorbent. Furthermore, for MIL101/ Alg, the peak at 3213 cm⁻¹ disappeared in the used adsorbent spectra. The peak alteration in zone I for the adsorbent used can be attributed to the attachment of Pi groups on the available O-H groups, which is one of the mechanisms that often occurs in the adsorption process of Pi with adsorbents having O-H groups [6]. The decrease in intensity for the peak related to O-H groups occurred due to the reduced number of O-H groups after being substituted with Pi. The zone II peaks indicate the presence of carboxylate groups in the adsorbents at \sim 1600 and \sim 1400 cm⁻¹, corresponding to ν (C=O) and ν s(COO⁻), respectively. The ν (C=O) was detected at a higher wavenumber of 1701 and 1688 cm⁻¹ for the fresh and used MIL101, respectively. At Zone III, the absorption peaks corresponding to the $\delta(O-H)$ and $\nu(C-O)$ vibration can be detected at \sim 1300 and \sim 1100 cm⁻¹, respectively. The absorption peaks associated with P-containing groups are also expected to appear within this zone [36,37]; thus, the peaks may have overlapped and are indistinguishable. Similarly, the absorption peak at Zone V (\sim 800 cm⁻¹) represents the occurrence of $\delta(C-H)$ and $\delta(P-O)$. Meanwhile, the peak

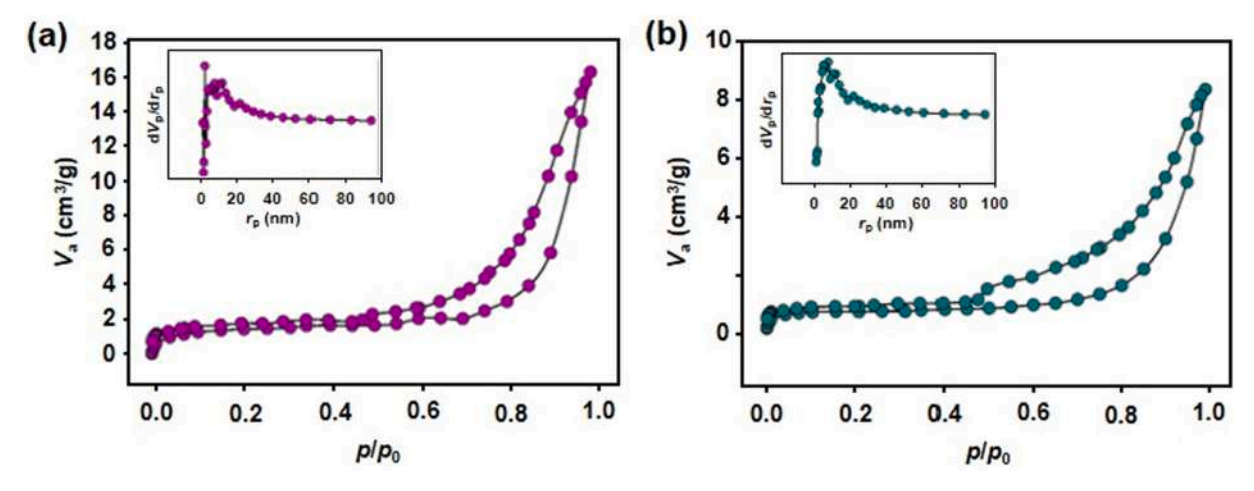


Fig. 1. N₂ sorption isotherm and the pore size distribution of (a) MIL100/Alg and (b) MIL101/Alg.

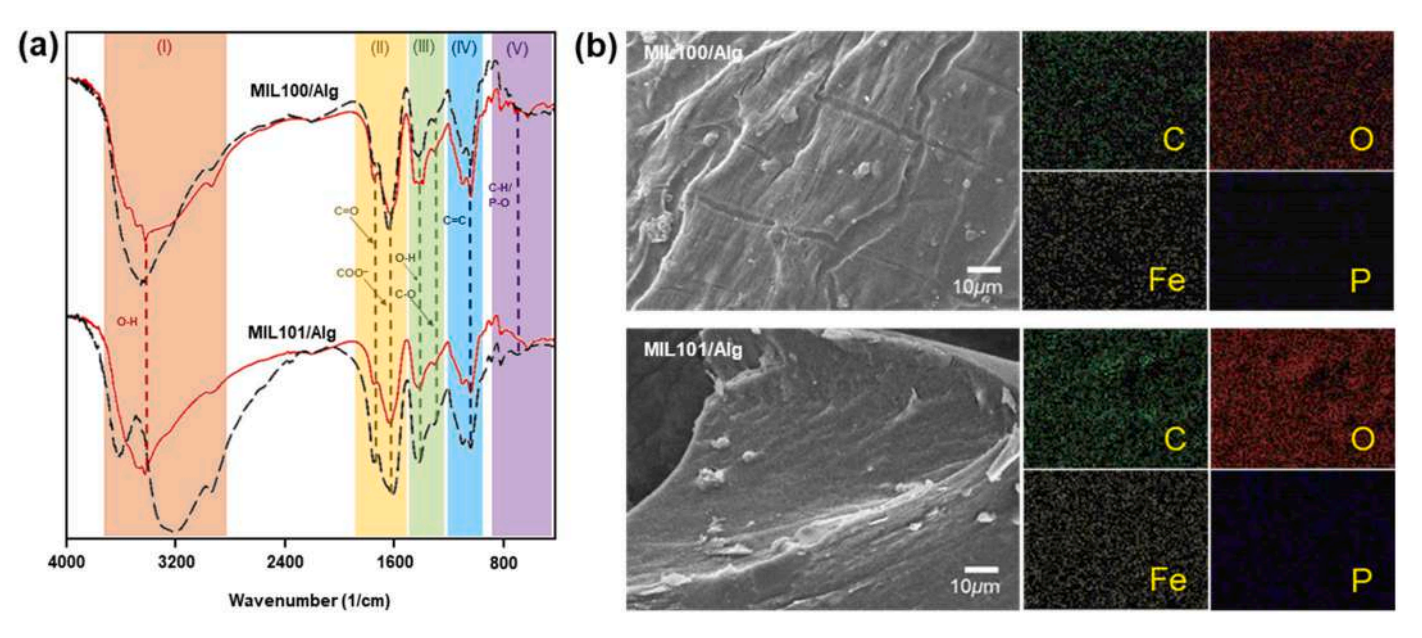


Fig. 2. (a) FTIR spectrum and (b) SEM image of MIL100/Alg and MIL101/Alg. The FTIR spectrum was recorded for the fresh adsorbent (——-, black dashed line) and post-adsorption (——, red solid line). The SEM image and corresponding elemental mapping were provided for the used adsorbent.

at zone IV corresponds to the $\delta(O\!-\!H)$ of the adsorbent, which is detected at $\sim\!1030~\text{cm}^{-1}.$

3.1.4. Morphology of the adsorbents

Electron micrographs of MIL100/Alg and MIL101/Alg (Fig. 2b) were obtained to observe the adsorbent morphology. The image of unmodified MIL100, MIL101, and Alg is provided in Fig. S4. The MIL100

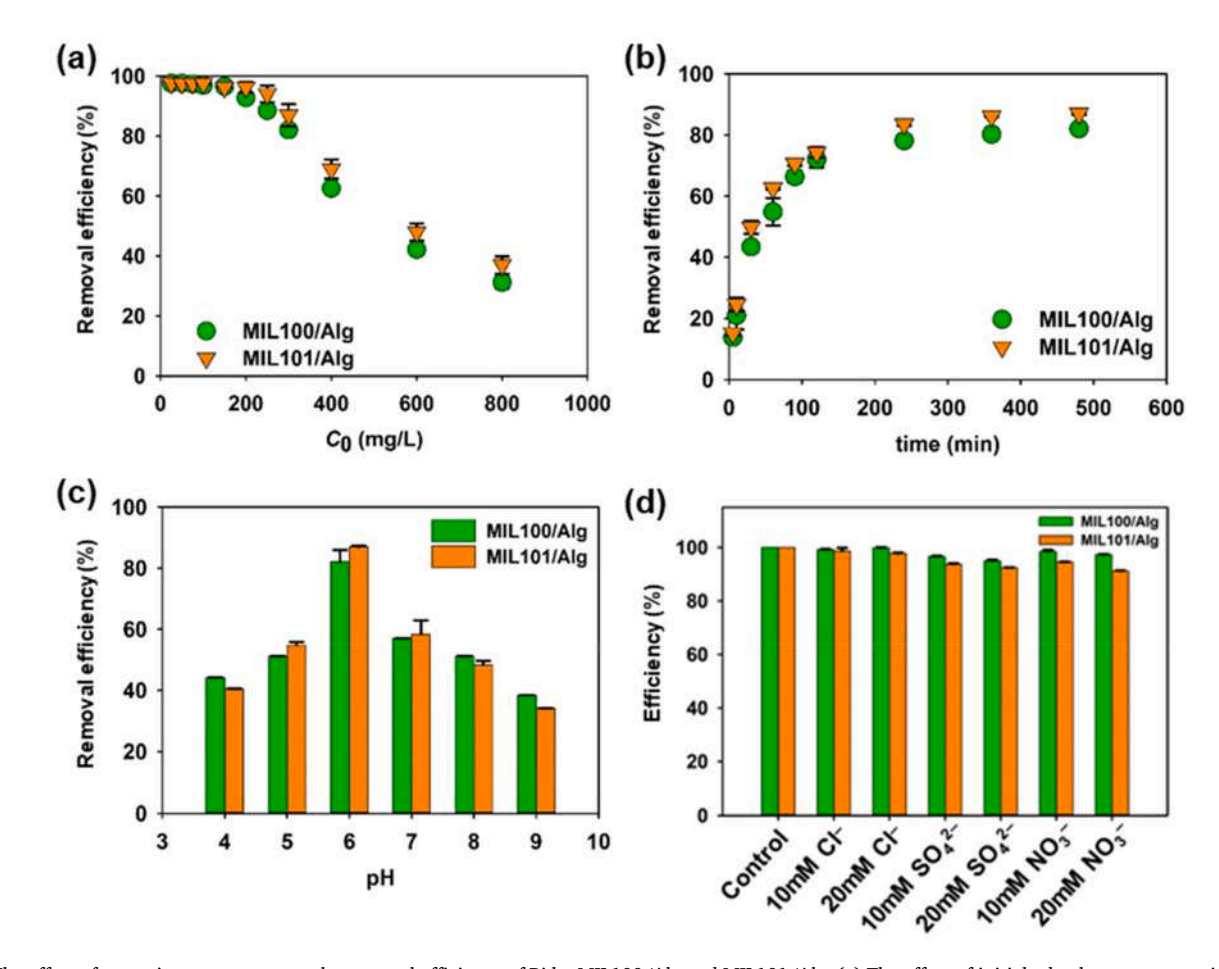


Fig. 3. The effect of operating parameters on the removal efficiency of Pi by MIL100/Alg and MIL101/Alg. (a) The effect of initial adsorbate concentration (C_0), (b) the effect of contact time, (c) the effect of pH, and (d) the decrease of removal efficiency in the presence of coexisting ions.

consists of a large number of particles with a typical octahedron shape, while only a small number of octahedron-shaped particles can be observed for MIL101. Alg shows a rigid and nonporous surface, which indicates the successful gelation of alginate molecules with Fe³⁺; the rigid structure of Alg also can be due to the extended gelation of alginate [38]. The surface of MIL100/Alg and MIL101/Alg (Fig. 2b) appears to be coarser than Alg (Fig. S4c'), which can be attributed to the change in the gelation of Alg due to the addition of MIL100 and MIL101 [24]. The EDX elemental mapping of the adsorbent after adsorption revealed the presence of P elements on the surface of the adsorbent, which confirmed the successful adsorption of Pi. Quantitative EDX analysis results (Fig. S5) indicate that the P loadings at MIL100, MIL101, Alg, MIL100/ Alg, and MIL101/Alg are approximately 0.20, 0.20, 0.14, 0.44, and 0.29 % atoms, respectively. The MIL100/Alg and MIL101/Alg composites showed a higher P content than their constituting material, indicating that the composite materials have improved adsorption affinity or capacity for Pi.

3.2. Effect of operating parameters on Pi removal efficiency

3.2.1. Effect of initial adsorbate concentration

Fig. 3a shows the effect of initial adsorbate concentration (C_0) on the removal efficiency of Pi by MIL100/Alg and MIL101/Alg; the results for the other adsorbents (i.e., MIL100, MIL101, and Alg) were presented in Fig. S6. At low C_0 , the adsorbents can almost completely remove the available Pi, but this removal efficiency decreased as the C_0 was increased. This phenomenon is commonly attributed to the number of available adsorption sites for adsorption, especially when a fixed amount of adsorbent is added to the system [7]. At low C_0 , the number of available adsorption sites is more than enough to adsorb the available adsorbates. At high C_0 , the number of adsorbate molecules increases while the number of adsorption sites remains the same; thus, more adsorbate is left unadsorbed.

3.2.2. Effect of contact time

At a C_0 of 300 mg/L and an adsorbent dose of 2.5 g/L, the removal efficiency for Pi by MIL100/Alg and MIL101/Alg increased as adsorption time was increased (Fig. 3b). The data for other adsorbents are provided in Fig. S7. Rapid adsorption of Pi occurs in the first 120 min, which was marked by a steep increase in removal efficiency. This happens because the adsorption sites of the adsorbent are still vacant so that the incoming adsorbate molecules can be instantaneously adsorbed. Furthermore, at the beginning of adsorption, the solute concentration in the bulk solution is higher than at the adsorbent surface, this concentration gradient being the driving force for the adsorption. A gradual increase in removal occurred after 120 min, indicating a near-equilibrium condition —At this point, the adsorbent is almost saturated because adsorbate molecules occupy most adsorption sites.

Swelling of MIL100/Alg and MIL101/Alg is observed to occur together with Pi uptake, which could be correlated with the increase in their removal efficiency of Pi. The swelling behavior of MIL100/Alg and MIL101/Alg is presented in Supplementary Information Fig. S10. The dry composite adsorbents (approximately 2.4 mm in size) showed ~1.4 times increase in size upon immersion in water. This is due to the water absorption ability of the hydrogel, which allows a certain number of water molecules to be retained. The Alg can achieve 120 % swellability (or 20 % swelling) after 480 min immersion in water. The addition of MOF particles allows higher swellability of the hydrogel, that is, 140 % and 134 % for MIL100/Alg and MIL101/Alg, respectively. The presence of MOF particles might be attributed to the inner pore enlargement, allowing more water molecules to be retained. After one day of immersion, there was no significant increase in swelling. The material could maintain its shape during immersion without breaking, implying the good mechanical strength of the adsorbents. The considerable swelling of the adsorbent occurred within the first 120 min of immersion, which coincided with a substantial increase in Pi uptake. The

uptake of Pi slows down as the swelling of the adsorbent has reached its optimum, i.e., after 120 min. This phenomenon might be attributed to the pore expansion of MIL 100/Alg and MIL 101/Alg during swelling, which allows Pi to enter the adsorbent and interact with the adsorption sites on their internal matrix.

3.2.3. Effect of initial pH

Pi is a pH-dependent compound that exists as different anionic species at different pH, affecting its adsorption behavior. Pi dominantly exists as H_3PO_4 at pH <2, as $H_2PO_4^-$ at pH 4-6, as HPO_4^{2-} at pH 8-9, and dominantly as PO₄³⁻ at highly alkaline pH. The pH effect on Pi removal efficiency was evaluated from the batch experiments in the pH range of 4–9 at C_0 of 300 mg/L and adsorbent dose of 2.5 g/L. It is observed that the highest Pi removal by MIL100/Alg and MIL101/Alg could be achieved at pH 6 (Fig. 3c); the removal efficiency is low at other pHs. Such behavior can be explained by the change in the adsorbent surface charge, which is also pH-dependent. The point-of-zero charge (PZC) of MIL100/Alg and MIL101/Alg is 6.51 and 6.63, respectively (Fig. S11). At pH 6, where the highest uptake of Pi occurred, the surface charge of MIL100/Alg and MIL101/Alg tended to be positive as the solution pH was below their PZCs. Therefore, the electrostatic attraction occurred between the positively charged adsorbent and negatively charged Pi in the form of H₂PO₄. At pH >6, MIL100/Alg and MIL101/Alg are negatively charged as the solution pH is higher than PZC, resulting in repulsive interactions due to the same charge of the adsorbent and adsorbate. Furthermore, a high pH would lead to the deprotonation of the Alg, which would increase the negativity of the adsorbents. Meanwhile, at low pH, Pi molecules in H₃PO₄ form may still prevail and coexist with H₂PO₄, thereby reducing electrostatic interactions [17,39]. In addition, it is worth noting that the removal efficiency of Pi by MIL100 and MIL101 were relatively constant in the wide pH range of 5-8, as shown in Supplementary Fig. S8a and b, indicating the low sensitivity of MIL100 and MIL 101 to pH variation.

The uptake of Pi by MIL100/Alg and MIL101/Alg could also be affected by the stability of the adsorbent at specific solution pH. The stability of MIL100/Alg and MIL101/Alg at a broad pH range was evaluated by immersing the adsorbents in a pH-adjusted solution for one day. There were no significant color changes in the materials upon immersion in solution at pH 4 to 10, implying that the materials were stable in this pH range. Meanwhile, at basic pH, the materials were found to be dissolved in the solution. The brownish color of the hydrogels disappeared upon immersion in pH 2 and 3 solutions (Fig. S11f), which can be attributed to the leaching of Fe³⁺ in an acidic environment. Nevertheless, a more detailed study will be required to explain this phenomenon.

3.2.4. Effect of coexisting ions

The effect of coexisting ions was studied to evaluate the selectivity of the adsorbent to Pi because the actual wastewater generally contains a mixture of various coexisting ions. The coexisting ions effect on the removal efficiency of Pi was studied by adding anions of Cl^- , SO_4^2 , and NO_3^- at approximately five- and ten-fold molar levels of Pi (2.1 mM as 200 mg $\text{PO}_4^{3-}/\text{L}$). These anionic ions were chosen as the competing adsorbate since Pi exists as an anion in the liquid phase, and it is postulated that a similar charge adsorbate caused more significant interference in the adsorption process.

The removal efficiency of Pi by MIL100/Alg and MIL101/Alg was not affected in the presence of Cl $^-$, SO $_4^2$, and NO $_3^-$ as competing ions (Fig. 3d). Similar behavior was also observed for Alg, MIL100, and MIL101 (Fig. S9). The decrease in Pi removal was $<10\,\%$ in the presence of the competitor ions. It was noted that the presence of SO $_4^2$ resulted in a slightly higher reduction in efficiency; this could be explained according to Helfferich's electro-selectivity concept, where the counter ions with higher valence tend to have greater affinity toward the adsorbent [39–42]. Ion strength at 20 mM significantly influences Pi removal efficiency because the competing ions are present at higher

numbers at higher molar concentrations. Nevertheless, the decrease in removal efficiency of Pi is still <10 %, indicating the excellent selectivity of the adsorbents toward Pi.

3.3. Adsorption studies

3.3.1. Adsorption equilibrium isotherm

The non-linear fittings (using selected isotherm models) on the Pi adsorption data onto Alg/Fe-MOF derived adsorbents at a constant temperature of 30 °C are shown in Fig. 4, and the corresponding parameters of the models are presented in Table 1. The investigated adsorption systems show a type L curve based on the classification by Giles et al. [43], which is commonly found in the aqueous phase adsorption systems. The L-type curve also indicates that the adsorbate molecules are adsorbed flat on the surface of the adsorbent. The long plateau forming at high $C_{\rm e}$ (i.e., > 100 mg/L) suggests the absence of the intermolecular interaction between the adsorbed molecules, and the saturation of the adsorbent has occurred. The steep increase in $Q_{\rm e}$ at low $C_{\rm e}$ (i.e., < 100 mg/L) indicates the high affinity of the adsorbate with the adsorbents at this stage —The increase of $Q_{\rm e}$ at this stage appears to be delayed for MIL100 and MIL101 when compared to MIL100/Alg and

MIL101/Alg (see Fig. S12), as implied by the less steep increase in $Q_{\rm c}$. This indicates that MIL100 and MIL101 have a lower affinity toward Pi than MIL100/Alg and MIL101/Alg.

Langmuir and Freundlich isotherm models were employed to evaluate the heterogeneity of the adsorption systems; the two models correlate most of the adsorption of water contaminants. In the adsorption of Pi using MIL100/Alg and MIL101/Alg, the Langmuir isotherm model was found to fit the adsorption data better than the Freundlich isotherm model, as implied by the higher R^2 and lower RSS. The suitability of the data to the Langmuir model implies a low heterogeneity of the adsorption sites. The maximum adsorption capacity of MIL100/Alg and MIL101/Alg toward Pi was found to be 103.3 and 109.5 mg/g, respectively. The maximum adsorption capacity of MIL100/Alg and MIL101/Alg compared with the other Fe-MOFs and alginate adsorbents was shown in Table 2, where the adsorbents in this study are found to have greater Pi adsorption capacity than most of the reported adsorbents.

The maximum adsorption capacity of the Frumkin-Fowler-Guggenheim model $(Q_{\rm FFG})$ was found to perfectly match the Langmuir adsorption capacity $(Q_{\rm L})$, which further confirms the suitability of the adsorption data to the Langmuir isotherm. The distribution of the heat of

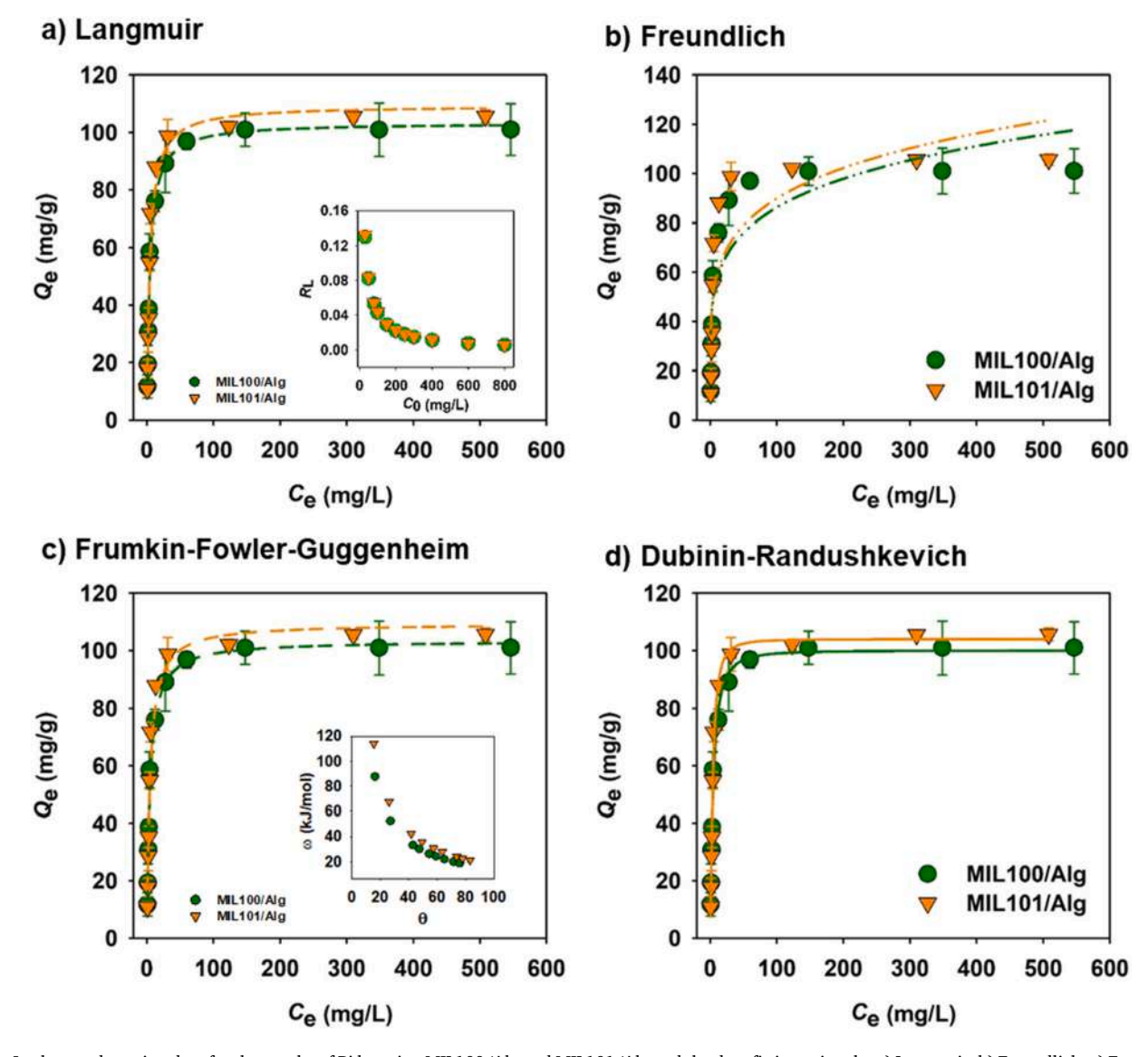


Fig. 4. Isotherm adsorption data for the uptake of Pi by using MIL100/Alg and MIL101/Alg and the data fitting using the a) Langmuir, b) Freundlich, c) Frumkin, and d) Dubinin-Randushkevich model. The adsorption was performed at 30 °C, an adsorbent dose of 2.5 g/L, and a pH of 6.

Table 1Parameter of Langmuir, Freundlich, Frumkin, and Dubinin-Randushkevich for the adsorption of Pi using MIL100/Alg and MIL101/Alg.

Parameter	Type of adsorbent	
	MIL100/Alg	MIL101/Alg
Langmuir		
$Q_{\text{L.max}} (\text{mg/g})$	103.3 ± 1.9	109.5 ± 3.8
$K_{\rm L}$ (L/mg)	0.223 ± 0.019	0.218 ± 0.030
R^2	0.989	0.966
RSS	126.9	422.1
Freundlich		
$K_{\rm F} ({\rm mg/g})({\rm mg/L})^{-n_{\rm F}}$	37.06 ± 6.72	38.04 ± 7.55
$n_{ m F}$	5.455 ± 1.112	5.365 ± 1.202
R^2	0.757	0.702
RSS	2718	3714
Dubinin-Randushkevich		
Q _{DR} (mg/g)	101.4 ± 8.3	104.0 ± 1.9
$B_{\rm DR} ({\rm mol}^2/{\rm kJ}^2) \times 10^5$	5.780 ± 0.003	6.322 ± 0.004
E _{DR} (kJ/mol)	12.85	10.18
R^2	0.989	0.990
RSS	99.37	98.30
Frumkin		
Q _{FFG} (mg/g)	103.3 ± 3.4	109.5 ± 4.3
φ	0.183 ± 0.001	0.365 ± 0.003
K _{FFG} (L/mg)	0.185	0.151
R^2	0.987	0.962
RSS	126.9	422.2

Table 2Comparison of maximum adsorption capacity of Pi using different adsorbents.

Adsorbent	Maximum adsorption capacity (mg Pi/g)	Ref.
MIL-100(Fe)	93.6	[22]
MIL-101(Fe)	167.22	[45]
MIL-101(Fe)	107.70	[23]
Ce-doped MIL-100(Fe)	12.03	[46]
NH ₂ -MIL-101	124.38	[23]
Alginate/Al-containing residue	59.5	[47]
Alginate/goethite	110.4	[48]
Ca-alginate beads	1.4	[49]
Ca-alginate-dolomite beads	28.45	[50]
Fe-alginate beads	62.92	This
		study
MIL100	84.01	This
		study
MIL101	88.48	This
		study
MIL100/Alg	103.3	This
		study
MIL101/Alg	109.5	This
		study

adsorption can be evaluated from the ω parameter of the Frumkin-Fowler-Guggenheim model. The inset of Fig. 4c shows the heat of adsorption (ω) as the function of surface coverage (θ) . The value of ω was found to decrease with increasing θ , contributing to a decrease in the interaction between the adsorbent and adsorbate as the adsorbate molecules gradually occupied the adsorption sites. The ω of MIL100/Alg and MIL101/Alg was higher than that of other investigated systems (see Fig. S12e); this can be ascribed to the increased interaction between the adsorbent and adsorbate. The Dubinin-Randushkevich model was employed on the adsorption system to predict the sorption behavior. The $E_{\rm DR}$ parameter of this model corresponds to the mean free adsorption energy. Physical adsorption occurs as the $E_{\rm DR}$ < 8 kJ/mol, and chemical adsorption occurs as the $E_{\rm DR}$ shows a value between 8 kJ/mol and 16 kJ/

mol [44]. As shown in 1, the investigated systems show $E_{\rm DR}$ values between 8 kJ/mol and 16 kJ/mol, implying the chemisorption tendency of the system.

As previously described, the Langmuir isotherm model shows good suitability with the adsorption isotherm data; therefore, the model was further used to fit the isotherm data at different temperatures (i.e., 40 and 50 °C). Additionally, the effect of temperature on the Langmuir-predicted adsorption capacity ($Q_{L,max}$) of Pi by MIL100/Alg and MIL101/Alg was investigated, and the result is provided in Fig. S14. The $Q_{L,max}$ decreases as the temperature increases, implying the exothermic behavior of the system. This phenomenon can be attributed to the deprotonation of the adsorbent. Since the hydroxyl and carboxyl functional groups of the adsorbent are more readily deprotonated at high temperatures [24], the adsorbent becomes more negatively charged, resulting in a repulsive interaction between the Pi and the adsorbent.

3.3.2. Adsorption kinetics

A kinetic study on the adsorption process was carried out to evaluate the adsorption rate and uptake profile of Pi onto the adsorbents. Pseudofirst-order and pseudo-second-order models were fitted to the kinetic data to predict the mechanism(s) involved in the adsorption process. The resulting model parameters from the regression analysis for the kinetic data obtained using MIL100/Alg or MIL101/Alg as an adsorbent are summarized in Table 3. The resulting fit of the models is presented in Fig. 5. Curve fitting results for other adsorbents are provided in Figs. S13 and Table S4. Of these two models, pseudo-second-order can better describe the adsorption kinetics of all adsorbents investigated, with the

Table 3Parameter of Pseudo-first-order, Pseudo-second-order, Elovich, and intraparticle diffusion for the adsorption of Pi onto MIL100/Alg and MIL101/Alg.

Parameter	Type of adsorbent	
	MIL100/Alg	MIL101/Alg
Pseudo-first-order		
$Q_{\rm e,1}~({ m mg/g})$	109.5 ± 3.4	116.3 ± 3.3
k_1 (1/min)	0.026 ± 0.003	0.027 ± 0.003
R^2	0.965	0.971
RSS	299.0	279.0
Pseudo-second-order		
$Q_{\rm e,2}~({\rm mg/g})$	120.1 ± 4.3	130.8 ± 4.8
$k_2 \text{ (mg/g min)}$	0.036 ± 0.001	0.037 ± 0.001
R^2	0.998	0.997
RSS	10.93	3.986
Elovich		
R _E	0.171 ± 0.014	0.167 ± 0.016
R^2	0.984	0.979
RSS	0.009	0.012
Zone class.	II	II
Zone crass.	11	11
Intra-particle diffusion (IPD)		
$R_{ m i}$	0.169 ± 0.011	0.170 ± 0.012
R^2	0.956	0.942
RSS	0.029	0.037
Zone class.	III	III
IPD – First segment		
$k_{\rm p,1} ({\rm mg/g \; min^{1/2}})$	11.04 ± 0.92	12.25 ± 1.22
C _{i.1} (mg/g)	-3.039 ± 1.029	-3.729 ± 0.394
R ²	0.978	0.978
RSS	33.83	40.36
IPD – Second segment		
$k_{\mathrm{p,2}}~(\mathrm{mg/g~min}^{1/2})$	1.903 ± 0.602	1.795 ± 0.748
$C_{i,2}$ (mg/g)	76.47 ± 3.21	85.51 ± 7.32
R^2	0.917	0.932
RSS	36.16	25.82

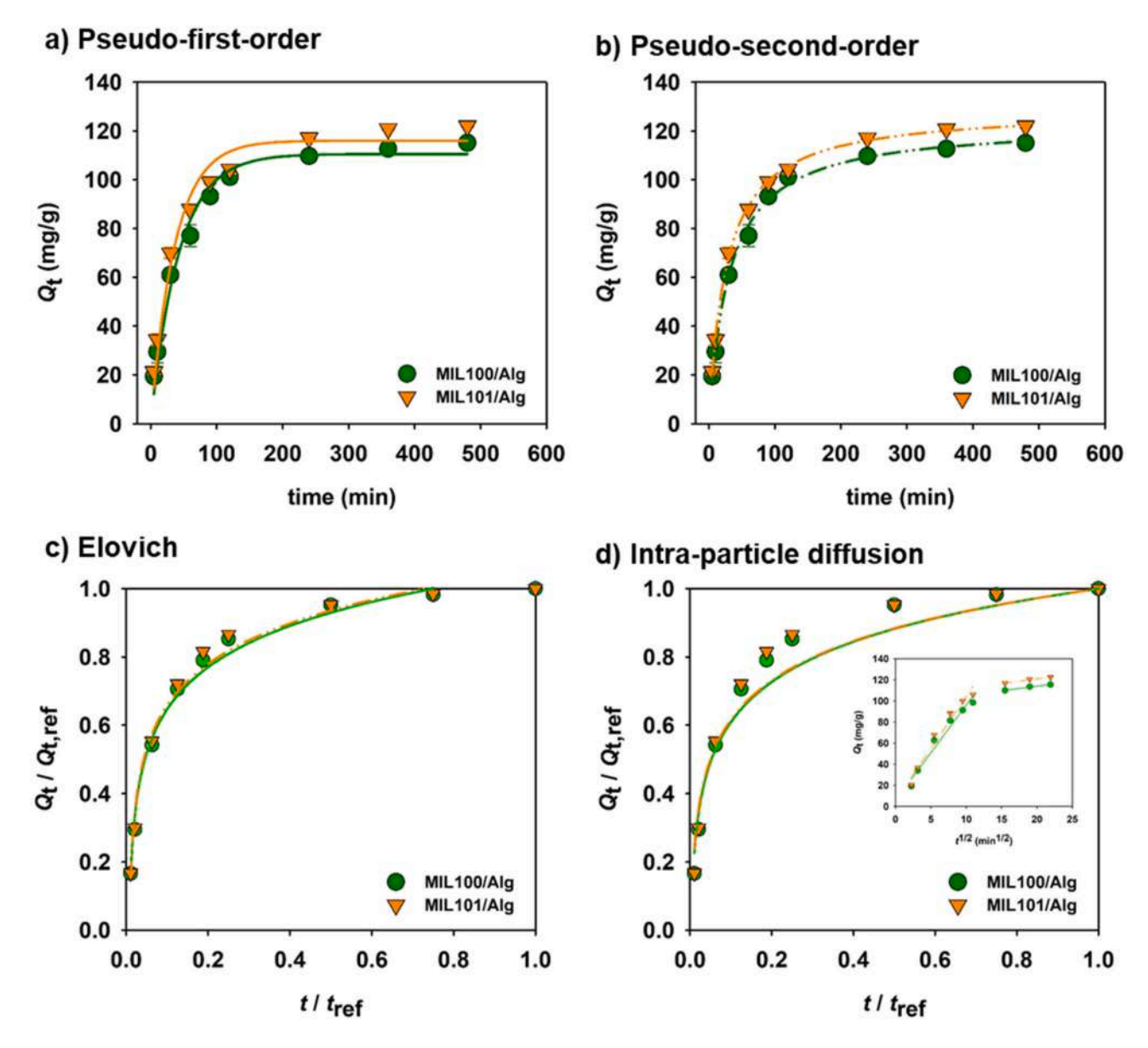


Fig. 5. Kinetic adsorption data for the uptake of Pi by using MIL100/Alg and MIL101/Alg and the data fitting using the (a) Pseudo-first-order, (b) Pseudo-second-order, (c) Elovich, and (d) Intra-particle diffusion model. The adsorption was performed at 30 °C, C₀ of 300 mg/L, an adsorbent dose of 2.5 g/L, and a pH of 6.

coefficient of determination (R^2) closer to 1. The better fit of pseudosecond-order with the kinetic data indicates that the adsorption process may involve chemisorption [6,51]. Based on the Pseudo-second-order adsorption rate (k_2) in Table 3, it can be noted that the addition of MIL100 or MIL101 promotes faster phosphate uptake for MIL100/Alg or MIL101/Alg compared to Alg alone. The slow adsorption rate of Alg can be attributed to its rigid and nonporous structure. Meanwhile, the faster adsorption of MIL100/Alg or MIL101/Alg could be due to the mesoporous structure (as revealed from the N_2 sorption isotherm characterization in Fig. 1), enabling the diffusion of the Pi molecules into the interior binding sites of the adsorbent, which lead to more efficient adsorption.

Elovich equation was employed in the kinetic data to evaluate the adsorption behavior that concurs with the chemical-driven adsorption system. The Elovich model fitting of the kinetic adsorption data is given in Fig. 5c. According to the value of $R_{\rm E}$ obtained from the non-linear regression of $(Q_{\rm t}/Q_{\rm t,ref})$ vs. $(t/t_{\rm ref})$, all adsorption systems belong to zone II of the mildly rising adsorption curve. This behavior is in good agreement with most chemical adsorption systems, which also fall into

zone II [52]. Following the Elovich model criteria of adsorption, a lower $R_{\rm E}$ value indicates faster adsorption kinetics in reaching equilibrium. MIL100 and MIL101, i.e., 0.152 and 0.171, exhibit more rapid Pi uptake than MIL101/Alg, MIL100/Alg, and Alg (0.167, 0.171, and 0.235, respectively). The difference in the uptake behavior could be due to the nonporous nature of Alg, which prevents the direct interaction of Pi with MIL100 and MIL101 particles so that the uptake rate slows down.

The dimensionless intra-particle diffusion (IPD) model was employed to evaluate the initial adsorption behavior of the investigated systems; the model fitting is shown in Fig. 5d. Based on the dimensionless R_i parameter in Table 3, all systems show a value of $0.5 > R_i > 0.1$, belonging to zone III of strong initial adsorption. The linear IPD model was fitted on the adsorption kinetic data to predict the initial diffusion rate; the model fitting was given as the inset of Fig. 5d and Supplementary Information Fig. S11e. All of the adsorbents exhibit two linear segments with different slopes. A steep slope was observed for the first segment, attributed to instantaneous adsorption on the surface of the adsorbent. The positive $C_{i,1}$ was observed for MIL100 and MIL101 (Table S4), suggesting rapid adsorption at the beginning and negligible

boundary layer effect [53]. The negative $C_{i,1}$ for Alg, MIL100/Alg, and MIL101/Alg (Table 3), suggests the non-negligible boundary layer effect; this could be attributed to the nonporous Alg matrix, which retarded the IPD. The rate constant of the first segment $(k_{\rm p,1})$ for MIL100/Alg and MIL101/Alg is faster than their single compartment. This implies that combining the MIL100 or MIL101 with Alg can promote Pi uptake, which can be associated with increased adsorption sites. With a slower rate constant, the second segment could be ascribed to the IPD-controlled gradual adsorption step. The $k_{\rm p,2}$ value shows that the rate constants of MIL100/Alg and MIL101/Alg are faster than MIL100 and MIL101, suggesting a higher adsorption affinity. It can be ascribed that the addition of Alg provides additional adsorption sites so that the saturation of the adsorbent can be delayed.

3.3.3. Adsorption mechanism

MIL100/Alg and MIL101/Alg adsorbents were prepared by combining MIL100 and MIL101 particles with Alg, followed by crosslinking using Fe³⁺ ions, providing MIL100/Alg and MIL101/Alg with three possible active sites. The first comes from their mesoporosity with uniform distribution of Fe active sites (as revealed from the EDX elemental mapping in Fig. 2). The second active sites are derived from the addition of MIL100 and MIL101, constructed from the complexation of Fe³⁺ and organic linkers. MIL100 and MIL101 can provide electrostatic attraction between positively charged metallic sites and anionic species of Pi. Besides electrostatic interaction, Pi can form a covalent bond with the metallic cation, inducing the ligand exchange phenomena [6,39]. The third adsorption site originated from the -OH group of Alg, where another ligand exchange phenomenon may occur [39]. Furthermore, the addition of crosslinked Alg aids in enriching the Fe³⁺ content in the adsorbent, as Alg binds the $\tilde{\text{Fe}^{3+}}$ ions along with the crosslinking process. Fig. 6 shows the schematic illustration of Pi adsorption using MIL100/Alg or MIL101/Alg adsorbent. The presence of coexisting anions does not significantly affect the adsorption of Pi; and is, therefore, not included in the illustration. The adsorbent swells upon immersion in a Pi-containing solution as the water molecules are absorbed along with Pi. The swelling of the adsorbent allows Pi to enter the interior of the adsorbent and interact with the active sites on the inner matrix, in addition to interacting with the active sites on the external surface. As Pi collides with the MIL100 or MIL101, the unsaturated -COO- coordinated Fe³⁺ serves as Lewis acid and attracts the lone pair electron of Pi via electrostatic attraction [39]. The presence of Fe³⁺ ions in the matrix of Alg also provides electrostatic attraction toward Pi, which further facilitates the adsorption.

3.4. Reusability study

Reusability is an essential property of an adsorbent which can show the cost-effectiveness of the adsorbent through repeated usage. According to the study on the effect of pH, the adsorbent has low adsorption at pH other than 6; thus, several eluents with different pH were used to determine the suitable eluent for regeneration of the adsorbents. It was found that ~90 % Pi could be removed by immersing used MIL100/Alg or MIL101/Alg in pH 9 solution with no significant physical change of the adsorbent; thus, the pH 9 solution was used as the adsorbent regeneration medium. The regenerated adsorbent was dried and applied for the successive adsorption-desorption cycle of Pi. It can be noted that there is no significant decrease in the Pi removal efficiency of the regenerated adsorbent after each cycle (Fig. S15a). MIL100/Alg and MIL101/Alg could maintain the Pi removal efficiency of >80 % of the original Pi removal for the subsequent cycles. This result implies that MIL100/Alg and MIL101/Alg can be regenerated and reused for Pi removal from the solution.

Furthermore, a simple Pi release study was carried out to provide an idea about the potential application of the spent adsorbent as a new atypical Pi source. The Pi-loaded adsorbent is immersed in water and placed in direct sunlight; this idea is based on a reported study where a polymer containing Fe³⁺ may undergo photoreduction to Fe²⁺ when exposed to direct (visible) light [54]. Here, we evaluate the possibility of releasing Pi during the reduction of Fe³⁺ to Fe²⁺. Upon 6 h of sunlight exposure, 1.2 to 1.8 mg/L of Pi can be released in the solution (Fig. S15b and c); meanwhile, almost no Pi can be released in the absence of incident light (data not shown here). Detailed future studies need to be conducted to determine the mechanism of Pi release due to this photoreduction effect.

In addition, an economic evaluation is carried out to estimate the cost required to produce each adsorbent. According to several reported economic studies, raw material procurement costs significantly contribute to direct operating costs (DOC). In this section, we evaluate DOC based on raw material requirements to produce the adsorbents on a kilogram-scale according to methods and steps demonstrated on a laboratory scale (refer to Section 2.2). The amount and cost of raw materials for sodium alginate, metal salt, organic linker, and solvent required for the production of each adsorbent are presented in Table S5. The cost evaluation results indicated that the production cost per kg of MIL100 and MIL101 was \sim 3 and \sim 5 times higher than that of the MIL100/Alg and MIL101/Alg composites, respectively. This further highlights the affordability and suitability (in terms of capacity and selectivity) of

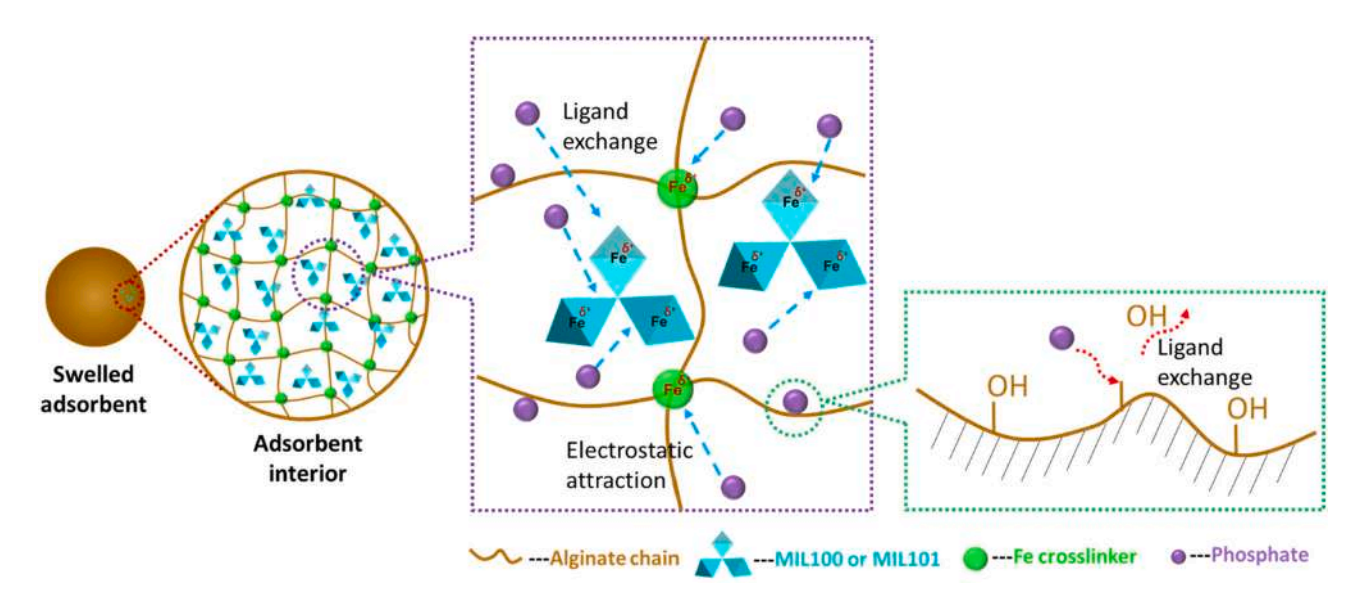


Fig. 6. Schematic illustration of Pi removal by MIL100/Alg or MIL101/Alg adsorbent.

using MIL100/Alg and MIL101/Alg for Pi adsorption.

4. Conclusion

Fe-containing composite beads, namely MIL100/Alg and MIL101/ Alg, have been successfully prepared by incorporating Fe-based MOFs (MIL100 or MIL101) into Alginate (Alg). By employing the hard-soft acid-base principle as the rationale for designing Pi-attracting adsorbents, the MIL100/Alg and MIL101/Alg demonstrated adequate selectivity toward Pi over anions such as Cl⁻, SO₄²⁻, and NO₃. Combining the microporous MIL100 or MIL101 into the nonporous Alg beads caused the formation of meso- and microporous structures in the beads, thus promoting their capacities. Additionally, the swellability of the Alg network accommodates the access of Pi anions to the adsorption sites (Fe) in the internal matrix of the adsorbent, where electrostatic attraction and ligand exchange between Pi and the Fe cation may take place. The MIL100/Alg and MIL101/Alg showed a high adsorption capacity of Pi (103.3 mg/g and 109.5 mg/g, respectively) at an aqueous solution pH 6, comparable or superior to other previously developed adsorbents. These capacities are approximately 1.7- to 1.2-fold higher than single adsorbents MIL100, MIL101, and Alg bead. The release of Pi from postadsorption adsorbent can easily be achieved by changing the solution pH, thus simplifying the reusability step. Amid 3 adsorption-desorption cycles, the adsorbents can maintain >80 % of their maximum capacity for Pi uptake. Economic evaluation on the production of beads suggests that compositing Alg and MIL100 or MIL101 may reduce the cost burden for MILs adsorbent without sacrificing the adsorption ability of the material. The possible application of Pi-loaded MIL100/Alg and MIL101/Alg as an atypical Pi source has been demonstrated modestly; further studies are needed to reveal the mechanism and evaluate the influencing parameters.

CRediT authorship contribution statement

Eric Alvares & Stanley Tantoro: Data Curation, Data analysis, Writing – Original Draft.

Christian Julius Wijaya: Data Curation, Formal analysis, Writing – Reviewing and Editing.

Kuan-Chen Cheng: Supervision, Conceptualization, Project administration.

Felycia Edi Soetaredjo: Project administration, Data analysis.

Hsien-Yi Hsu & Chang-Wei Hsieh: Project administration; Resources.

Artik Elisa Angkawijaya: Conceptualization, Formal analysis, Writing – Reviewing and Editing.

Alchris Woo Go: Project administration, Writing – Reviewing and Editing.

Shella Permatasari Santoso: Supervision, Conceptualization, Resources, Project administration, Funding acquisition.

Declaration of competing interest

The authors declare that they have no known competing financial interests or personal relationships that could have appeared to influence the work reported in this paper.

Data availability

Data will be made available on request.

Acknowledgments

The authors acknowledge the financial support by the Science and Technology Innovation Center for Circular Economy and Green Innovative Resources (STIC-CEGIR) and Widya Mandala Surabaya Catholic University.

Appendix A. Supplementary data

Supplementary data to this article can be found online at https://doi.org/10.1016/j.jjbiomac.2023.123322.

References

- [1] H.P. Schwarcz, 14.22 Human Physiology in Relation to Isotopic Studies of Ancient and Modern Humans, in: H.D. Holland, K.K. Turekian (Eds.), Treatise on Geochemistry, Second Edition, Elsevier, Oxford, 2014, pp. 357–369.
- [2] R. Thuynsma, A. Kleinert, J. Kossmann, A.J. Valentine, P.N. Hills, The effects of limiting phosphate on photosynthesis and growth of Lotus japonicus, S. Afr. J. Bot. 104 (2016) 244–248.
- [3] M.M. Mekonnen, A.Y. Hoekstra, Global anthropogenic phosphorus loads to freshwater and associated Grey water footprints and water pollution levels: a highresolution global study, Water Resour. Res. 54 (2017) 345–358.
- [4] X. Chen, Y. Wang, Z. Bai, L. Ma, M. Strokal, C. Kroeze, X. Chen, F. Zhang, X. Shi, Mitigating phosphorus pollution from detergents in the surface waters of China, Sci. Total Environ. 804 (2022), 150125.
- [5] J. Wang, D. Chen, B. Li, J. He, D. Duan, D. Shao, M. Nie, Fe-MIL-101 exhibits selective cytotoxicity and inhibition of angiogenesis in ovarian cancer cells via downregulation of MMP, Sci. Rep. 6 (2016) 26126.
- [6] P. Zhang, M. He, S. Huo, F. Li, K. Li, Recent progress in metal-based composites toward adsorptive removal of phosphate: mechanisms, behaviors, and prospects, Chem. Eng. J. 446 (2022), 137081.
- [7] A.E. Angkawijaya, S.P. Santoso, V. Bundjaja, F.E. Soetaredjo, C. Gunarto, A. Ayucitra, Y.-H. Ju, A.W. Go, S. Ismadji, Studies on the performance of bentonite and its composite as phosphate adsorbent and phosphate supplementation for plant, J. Hazard. Mater. 399 (2020), 123130.
- [8] H. Xiong, S. Peng, D. Zhang, Phosphate adsorption removal by (La-doping) Mn–Al bimetal oxide composites, Mater. Chem. Phys. 285 (2022), 126195.
- [9] M. Langer, J. Väänänen, M. Boulestreau, U. Miehe, C. Bourdon, B. Lesjean, Advanced phosphorus removal via coagulation, flocculation and microsieve filtration in tertiary treatment, Water Sci. Technol. 75 (2017) 2875–2882.
- [10] M.R. Awual, A.M. Asiri, M.M. Rahman, N.H. Alharthi, Assessment of enhanced nitrite removal and monitoring using ligand modified stable conjugate materials, Chem. Eng. J. 363 (2019) 64–72.
- [11] M.R. Awual, A. Jyo, Rapid column-mode removal of arsenate from water by crosslinked poly(allylamine) resin, Water Res. 43 (2009) 1229–1236.
- [12] M.R. Awual, M.A. Shenashen, T. Yaita, H. Shiwaku, A. Jyo, Efficient arsenic(V) removal from water by ligand exchange fibrous adsorbent, Water Res. 46 (2012) 5541–5550.
- [13] M.R. Awual, M.M. Hasan, A. Islam, M.M. Rahman, A.M. Asiri, M.A. Khaleque, M. C. Sheikh, Introducing an amine functionalized novel conjugate material for toxic nitrite detection and adsorption from wastewater, J. Clean. Prod. 228 (2019) 778–785
- [14] R.M. Kamel, A. Shahat, W.H. Hegazy, E.M. Khodier, M.R. Awual, Efficient toxic nitrite monitoring and removal from aqueous media with ligand based conjugate materials, J. Mol. Liq. 285 (2019) 20–26.
- [15] M.R. Awual, T. Yaita, S. Suzuki, H. Shiwaku, Ultimate selenium(IV) monitoring and removal from water using a new class of organic ligand based composite adsorbent, J. Hazard. Mater. 291 (2015) 111–119.
- [16] M.R. Awual, A. Jyo, T. Ihara, N. Seko, M. Tamada, K.T. Lim, Enhanced trace phosphate removal from water by zirconium(IV) loaded fibrous adsorbent, Water Res. 45 (2011) 4592–4600.
- [17] M.R. Awual, Efficient phosphate removal from water for controlling eutrophication using novel composite adsorbent, J. Clean. Prod. 228 (2019) 1311–1319.
- [18] M.R. Awual, M.A. Shenashen, A. Jyo, H. Shiwaku, T. Yaita, Preparing of novel fibrous ligand exchange adsorbent for rapid column-mode trace phosphate removal from water, J. Ind. Eng. Chem. 20 (2014) 2840–2847.
- [19] M.R. Awual, A. Jyo, Assessing of phosphorus removal by polymeric anion exchangers, Desalination 281 (2011) 111–117.
- [20] M.R. Awual, A. Jyo, S.A. El-Safty, M. Tamada, N. Seko, A weak-base fibrous anion exchanger effective for rapid phosphate removal from water, J. Hazard. Mater. 188 (2011) 164–171.
- [21] A. Shahat, H.M.A. Hassan, H.M.E. Azzazy, M. Hosni, M.R. Awual, Novel nanoconjugate materials for effective arsenic(V) and phosphate capturing in aqueous media, Chem. Eng. J. 331 (2018) 54–63.
- [22] M. Nehra, N. Dilbaghi, N.K. Singhal, A.A. Hassan, K.-H. Kim, S. Kumar, Metal organic frameworks MIL-100(Fe) as an efficient adsorptive material for phosphate management, Environ. Res. 169 (2019) 229–236.
- [23] Q. Xie, Y. Li, Z. Lv, H. Zhou, X. Yang, J. Chen, H. Guo, Effective adsorption and removal of phosphate from aqueous solutions and eutrophic water by Fe-based MOFs of MIL-101, Sci. Rep. 7 (2017) 3316.
- [24] A. Andreas, Z.G. Winata, S.P. Santoso, A.E. Angkawijaya, M. Yuliana, F. E. Soetaredjo, S. Ismadji, H.-Y. Hsu, A.W. Go, Y.-H. Ju, Biocomposite hydrogel beads from glutaraldehyde-crosslinked phytochemicals in alginate for effective removal of methylene blue, J. Mol. Liq. 329 (2021), 115579.
- [25] P. Singh, S.K. Singh, J. Bajpai, A.K. Bajpai, R.B. Shrivastava, Iron crosslinked alginate as novel nanosorbents for removal of arsenic ions and bacteriological contamination from water, J.Mater.Res.Technol. 3 (2014) 195–202.
- [26] Y. Bai, Y. Zhao, Y. Li, J. Xu, X. Fu, X. Gao, X. Mao, Z. Li, UV-shielding alginate films crosslinked with Fe3+ containing EDTA, Carbohydr. Polym. 239 (2020), 115480.

- [27] K.Y. Lee, D.J. Mooney, Alginate: properties and biomedical applications, Prog. Polym. Sci. 37 (2012) 106–126.
- [28] C.C. Spadari, F. deBastiani, L.B. Lopes, K. Ishida, Alginate nanoparticles as non-toxic delivery system for miltefosine in the treatment of candidiasis and cryptococcosis, Int. J. Nanomedicine 14 (2019) 5187–5199.
- [29] M.A. Simon, E. Anggraeni, F.E. Soetaredjo, S.P. Santoso, W. Irawaty, T.C. Thanh, S. B. Hartono, M. Yuliana, S. Ismadji, Hydrothermal synthesize of HF-free MIL-100 (Fe) for isoniazid-drug delivery, Sci. Rep. 9 (2019) 16907.
- [30] F.E. Adelowo, S.O. Oladeji, Spectrophotometric analysis of phosphate concentration in agricultural soil samples and water samples using molybdenum blue method, <sb:contribution><sb:title>Braz. </sb:title></sb:contribution><sb:sissue><sb:series><sb:title>J. Biol. Sci.</sb:title></sb:title></sb:series></sb:shost></sb:shost>3 (2018), 4-7=412.
- [31] K.H. Chu, B.C. Tan, Is the Frumkin (Fowler–Guggenheim) adsorption isotherm a two- or three-parameter equation? Colloid Interface Sci.Commun. 45 (2021), 100519.
- [32] C.D. Sulistiyo, K.-C. Cheng, H.J. Su'andi, M. Yuliana, C.-W. Hsieh, S. Ismadji, A. E. Angkawijaya, A.W. Go, H.Y. Hsu, P.L. Tran-Nguyen, S.P. Santoso, Removal of hexavalent chromium using durian in the form of rind, cellulose, and activated carbon: comparison on adsorption performance and economic evaluation, J. Clean. Prod. 380 (2022), 135010.
- [33] N. Yao, Y. Zhang, R. Zhang, L. Zhang, D. Yue, One-step fabrication of HNBR/MIL-100 composites via selective hydrogenation of acrylonitrile-butadiene rubber with a catalyst derived from MIL-100(Fe), J. Mater. Sci. 56 (2021) 326–336.
- [34] H. Shi, Z. Gu, M. Han, C. Chen, Z. Chen, J. Ding, Q. Wang, H. Wan, G. Guan, Preparation of heterogeneous interfacial catalyst benzimidazole-based acid ILs@ MIL-100(Fe) and its application in esterification, Colloids Surf. A Physicochem. Eng. Asp. 608 (2021), 125585.
- [35] Y. Wang, W. Guo, X. Li, Activation of persulfates by ferrocene–MIL-101(Fe) heterogeneous catalyst for degradation of bisphenol A, RSC Adv. 8 (2018) 36477–36483.
- [36] D.H. Barnes, R. Jugdaosingh, S. Kiamil, S.M. Best, Shelf life and chemical stability of calcium phosphate coatings applied to poly carbonate urethane substrates, J. Biotechnol.Biomater. 1 (2011) 112.
- [37] E. Faulques, N. Kalashnyk, F. Massuyeau, D.L. Perry, Spectroscopic markers for uranium(vi) phosphates: a vibronic study, RSC Adv. 5 (2015) 71219–71227.
- [38] T. Jeoh, D.E. Wong, S.A. Strobel, K. Hudnall, N.R. Pereira, K.A. Williams, B. M. Arbaugh, J.C. Cunniffe, H.B. Scher, How alginate properties influence in situ internal gelation in crosslinked alginate microcapsules (CLAMs) formed by spray drying, Plos One 16 (2021), e0247171.
- [39] R. Liu, L. Chi, X. Wang, Y. Wang, Y. Sui, T. Xie, H. Arandiyan, Effective and selective adsorption of phosphate from aqueous solution via trivalent-metals-based amino-MIL-101 MOFs, Chem. Eng. J. 357 (2019) 159–168.

- [40] M.R. Awual, S.A. El-Safty, A. Jyo, Removal of trace arsenic(V) and phosphate from water by a highly selective ligand exchange adsorbent, J. Environ. Sci. 23 (2011) 1947–1954.
- [41] M.R. Awual, M.M. Hasan, A.M. Asiri, M.M. Rahman, Cleaning the arsenic(V) contaminated water for safe-guarding the public health using novel composite material, Compos.Part B 171 (2019) 294–301.
- [42] M.R. Awual, M.M. Hasan, T. Ihara, T. Yaita, Mesoporous silica based novel conjugate adsorbent for efficient selenium(IV) detection and removal from water, Microporous Mesoporous Mater. 197 (2014) 331–338.
- [43] J.S. Piccin, Tito Roberto Sant'Anna Cadava, L.A.A.d. Pinto, G.L. Dotto, A. Bonilla-Petriciolet, D.I. Mendoza-Castillo, H.E. Reynel-Avila (Eds.), Adsorption Isotherms in Liquid Phase: Experimental, Modeling, and Interpretations. Adsorption Processes for Water Treatment and Purification, Springer Nature, Switzerland, 2017.
- [44] Q. Hu, Z. Zhang, Application of Dubinin-Radushkevich isotherm model at the solid/solution interface: a theoretical analysis, J. Mol. Liq. 277 (2019) 646–648.
- [45] Y. Wu, Z. Liu, M.F. Bakhtari, J. Luo, Preparation of GO/MIL-101(Fe, Cu) composite and its adsorption mechanisms for phosphate in aqueous solution, Environ. Sci. Pollut. Res. 28 (2021) 51391–51403.
- [46] Z. Jiao, Z. Miao, H. An, Q. Li, X. Meng, Fabrication of Ce-doped MIL-100(Fe), its adsorption performance, and the mechanisms to adsorb phosphate from water, Environ. Technol. Innov. 28 (2022), 102847.
- [47] C. Shen, Y. Zhao, R. Liu, Y. Mao, D. Morgan, Adsorption of phosphorus with calcium alginate beads containing drinking water treatment residual, Water Sci. Technol. 78 (2018) 1980–1989.
- [48] H. Siwek, A. Bartkowiak, M. Włodarczyk, Adsorption of phosphates from aqueous solutions on alginate/goethite hydrogel composite, Water 11 (2019) 633.
- [49] Z. Isik, M. Saleh, N. Dizge, Adsorption studies of ammonia and phosphate ions onto calcium alginate beads, Surf.Interfaces 26 (2021), 101330.
- [50] Y.-X. Huang, M.-J. Liu, S. Chen, I.I. Jasmi, Y. Tang, S. Lin, Enhanced adsorption and slow release of phosphate by dolomite–alginate composite beads as potential fertilizer, Water Environ.Res. 91 (2019) 797–804.
- [51] H.K. Agbovi, L.D. Wilson, 1 adsorption processes in biopolymer systems: fundamentals to practical applications, in: S. Kalia (Ed.), Natural Polymers-Based Green Adsorbents for Water Treatment, Elsevier, 2021, pp. 1–51.
- [52] F.-C. Wu, R.-L. Tseng, R.-S. Juang, Characteristics of elovich equation used for the analysis of adsorption kinetics in dye-chitosan systems, Chem. Eng. J. 150 (2009) 366–373.
- [53] F.-C. Wu, R.-L. Tseng, R.-S. Juang, Initial behavior of intraparticle diffusion model used in the description of adsorption kinetics, Chem. Eng. J. 153 (2009) 1–8.
- [54] G.E. Giammanco, C.T. Sosnofsky, A.D. Ostrowski, Light-responsive iron(III) polysaccharide coordination hydrogels for controlled delivery, ACS Appl. Mater. Interfaces 7 (2015) 3068–3076.